Supporting Information for

Pyrolysis-Free Synthesized Single-Atom Cobalt Catalysts for Efficient Oxygen Reduction

Rui Ma,[a] Xun Cui,[a,b] Yonglin Wang,[a] Zongying Xiao,[a] Rui Luo,[a] Likun Gao,[d] Zhengnan Wei[e] and Yingkui Yang*[a,c]*

[a]Key Laboratory of Catalysis and Energy Materials Chemistry of Ministry of Education, Hubei Key Laboratory of Catalysis and Materials Science, South-Central University for Nationalities, Wuhan 430074, China.
E-mail: xcui@scuec.edu.cn; ykyang@mail.scuec.edu.cn

[b]Engineering Research Centre of Nano-Geomaterials of Ministry of Education, China University of Geosciences, Wuhan 430074, China.

[c]Hubei Engineering Technology Research Centre of Energy Polymer Materials, School of Chemistry and Materials Science, South-Central University for Nationalities, Wuhan 430074, China.

[d]Key Laboratory of Bio-based Material Science and Technology of Ministry of Education, Northeast Forestry University, Harbin 150040, China.

[e]New Energy Development Centre, Shengli Petroleum Administration Co., Ltd, SINOPEC, China.

The Supporting Information file includes:

1. Experimental Section

1.1 Materials

All starting materials and solvents, unless otherwise noted, were used as received. Commercial Pt/C (20%), thieno/thiophene-2,5-dicarboxaldehyde (bTDA) and Cobalt acetate tetrahydrate ($Co(CH_3COO)_2 \cdot 4(H_2O)$) were purchased from Sigma. 2,5-Thiophenedicarboxaldehyde (TDA) and o-dichlorobenzene (o-DCB) were purchased from Macklin. Tetraamine porphyrin (TPP) were purchased from Energy Chemical. Terephthalaldehyde (PPA) were acquired from Aladdin and other materials were purchased from Sinopharm Chemical Reagent Co. LTD.

1.2 Synthesis of PTS-COPs, PTS-COPs-1 and P-COPs

TPP (0.05 mmol, 33.8 mg) and bTDA (0.10 mmol, 9.8 mg) were combined in a glass container with a n-butanol/dichlorobenzene solution (1:1 V/V) and subjected 10 min of sonication. After the addition of 0.2 ml of 6 M acetic acid, the solution was heated to 120 ℃ for 72 h. Finally, the PTS-COPs solid was isolated by filtration and subsequently thoroughly washed and dried at 80 ℃ under vacuum. In a similar procedure, by replacing bTDA (0.10 mmol, 9.8 mg) with TDA (0.10 mmol, 14.1 mg) and PPA (0.1 mmol, 13.4 mg), respectively, PTS-COPs-1 and P-COPs can be obtained.

1.3 Synthesis of PTS-COPs@MWCNTs-x (x = 0.5, 1 and 2)

In a typical synthesis, 50 mg MWCNTs were first dispersed in 10 ml DMAC solvent to obtain a uniform MWCNTs dispersion. The TPP and bTDA with a molar ratio of 1:2 were then added in above dispersion. After the addition of 0.1 ml of 6 M acetic acid and 30 min of sonication, the mixtures were heated to 120 °C and maintained for 72 h under the condition of agitation and argon protection. Finally, the PTS-COPs@MWCNTs was obtained after filtration, thoroughly washing, and overnight drying under vacuum. The quantities of precursors (i.e., TPP and bTDA) can be adjusted to yield PTS-COPs@MWCNTs with different weight ratios between MWCNTs and PTS-COPs ($m_{monomers}/m_{MWCNTs}$ = 0.5, 1 and 2), thereby tuning the thickness of the PTS-COPs shell wrapped around the MWCNTs core. Therefore, a set of PTS-COPs@MWCNTs (denoted PTS-COPs@MWCNTs-x, where x refers to the mass ratio of 0.5, 1 and 2) can be readily obtained.

1.4 Synthesis of Co-PTS-COPs@MWCNTs

In a typical synthesis, $Co(CH_3COO)_2 \bullet 4(H_2O)$ and the optimal PTS-COPs@MWCNTs-1 with a mass ratio of 2:1 were mixed and stirred in a certain amount of ethanol solution. After 60 min of sonication, the mixture was heated to 60 °C for 12 h under the condition of agitation. Finally, the Co-PTS-COPs@MWCNTs can be obtained after filtration and thoroughly washing, and overnight drying under vacuum. To study the effect of Co content on the electrocatalytic ORR activity, the mass ratio of Co precursor/PTS-COPs@MWCNTs-1 was also adjusted to 1:1, 1.5:1, and 3:1, respectively.

1.5 Materials Characterization

The morphology was observed by SEM on an SU 8010 microscope. TEM images were acquired on a Hitachi HT7700 electron microscope. Powder XRD patterns were recorded on a Rigaku D/Max 2400 system using monochromatic Cu Kα X-ray source

radiation at a scanning speed of 0.1 s^{-1}. High-resolution TEM (HRTEM) images were obtained using a TECNAIG2 F30 operated at 200 kV. EDX measurements were performed to verify the chemical composition and distribution. The surface composition was analyzed through XPS, using a Thermo K-alpha photoelectron spectrometer with Al Kα radiation as the excitation source. Raman scattering spectra were recorded on a Renishaw System 2000 spectrometer. HAADF-STEM images were recorded on a JEOL-2100F FETEM with electron acceleration energy of 200 kV. Fourier transform infrared spectroscopy (FT-IR) spectra were obtained using a Thermo Nicolet NEXUS 470 in the wavenumber range of 4000-500 cm^{-1}. XAFS spectra at the Co K-edge (7709 eV) was collected at BL14W1 station at Shanghai Synchrotron Radiation Facility (SSRF). Co foil, CoPc, CoO, and Co_3O_4 were used as references.

1.6 Electrochemical Measurements

The electrochemical measurements were carried out using the CHI 760E potentiost in a general three-electrode system, in which Ag/AgCl (saturated KCl) regarded as the reference electrode, graphite rod as the counter electrode, and 0.1 M KOH aqueous solution as electrolyte. All the potentials in this work were converted to the reversible hydrogen electrode (RHE) according to the Nernst equation ($E_{RHE} = E_{(Ag/AgCl)} + 0.0591 \times pH + 0.197$). A rotating disk electrode (glassy carbon; 5.0-mm diameter) coated with catalyst film was used as the working electrode. The catalyst ink was prepared by dispersing 5 mg of catalyst powder with 1 mL water-ethanol-Nafion (5 wt%) (v/v/v = 13/6/1) mixed solvent by sonication for 30 min. The loading amounts of all the catalysts including commercial Pt/C (20 wt%) were 0.2 mg cm^{-2}. Before tests, the electrolyte was saturated with N_2/O_2 by bubbling N_2/O_2 into the container for at least 30 min. The cyclic voltammetry (CV) tests were conducted in N_2- and O_2-saturated electrolyte solutions with a sweep rate of 25 mV s^{-1}. The LSV tests were performed in O_2-saturated electrolyte solutions at different rotating speeds from 400 to 1600 rpm (American Pine Instruments device) with a scan rate of 5 mV s^{-1}. The long-term durability tests were conducted by chronoamperometry at the half-wave potential for 36 000 s in O_2-saturated electrolyte with a rotation speed of 1600 rpm. The values of electron transfer number (n) were calculated using the Koutecky-Levich equation:

$$\frac{1}{j} = \frac{1}{j_L} + \frac{1}{j_K} = \frac{1}{B\omega^{1/2}} + \frac{1}{j_K}$$

$$B = 0.2nFAC_0D_0^{2/3}v^{-1/6}$$

where j, j_L, and j_K are the measured current density, limiting current density, and kinetic current density, respectively, ω is the rotating speed (angular velocity), n is the electron transfer number, F is the Faraday constant (96 485 C mol^{-1}), C_0 is the bulk concentration of O_2 (1.2×10^{-3} mol L^{-1}), D_0 is the diffusion coefficient of O_2 (1.9×10^{-5} cm^2 s^{-1}), and υ is the kinematic viscosity of the electrolyte (0.01 cm^2 s^{-1}). The rotating ring disk electrode (RRDE) measurements were performed to calculate the yield of H_2O_2 and electron transfer number (n) according the following equations:

$$H_2O_2\% = 200 \frac{Ir/N}{Id+Ir/N}$$

$$n = 4 \frac{I_d}{I_d+Ir/N}$$

where I_r is the ring current, I_d is the disk current, and N is the collection efficiency of the Pt ring (N = 0.37, provided by the manufacturer).

2. Figures

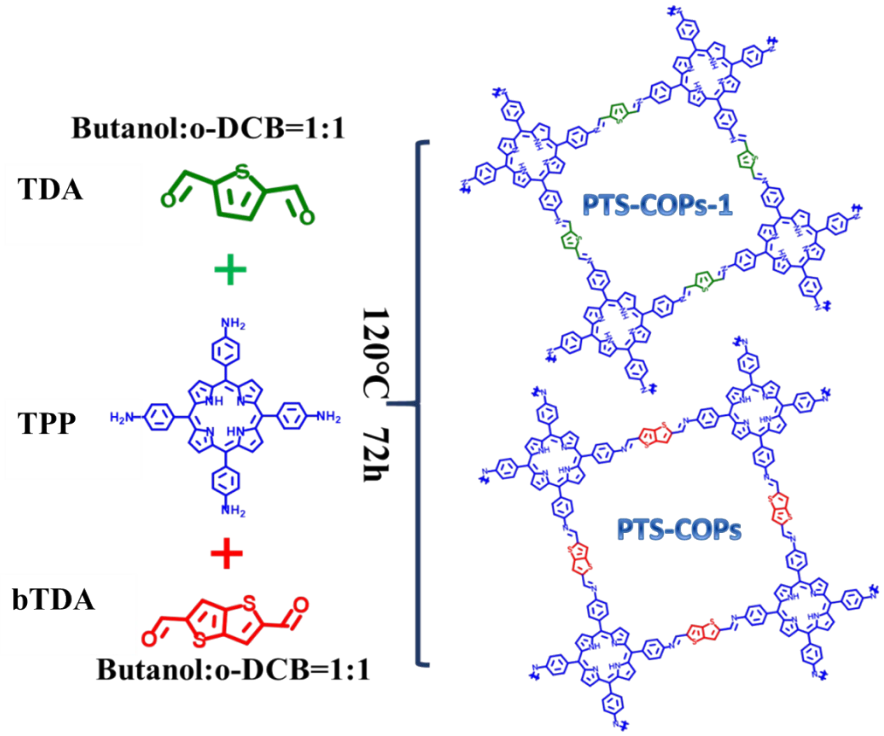

Figure S1. Schematic illustration for the synthesis of PTS-COPs and PTS-COPs-1 with the absence of MWCNTs.

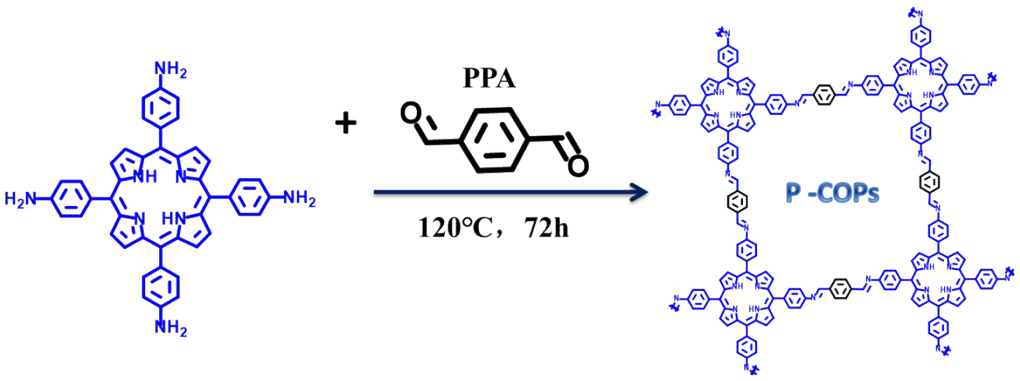

Figure S2. Schematic illustration for the synthesis of P-COPs with the absence of MWCNTs.

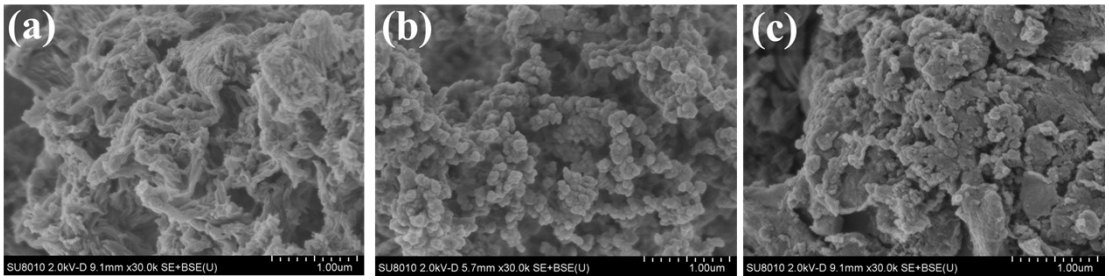

Figure S3. SEM images of the as-synthesized (a) PTS-COPs, (b) PTS-COPs-1 and (c) P-COPs.

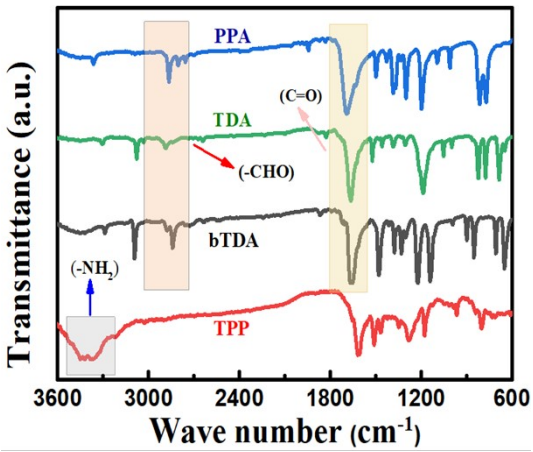

Figure S4. FTIR spectra of the monomers (PPA, TDA, bTDA, and TPP).

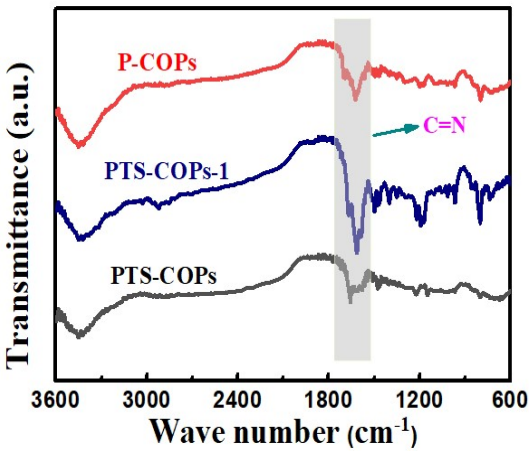

Figure S5. FTIR spectra of the as-synthesized PTS-COPs, PTS-COPs-1 and P-COPs.

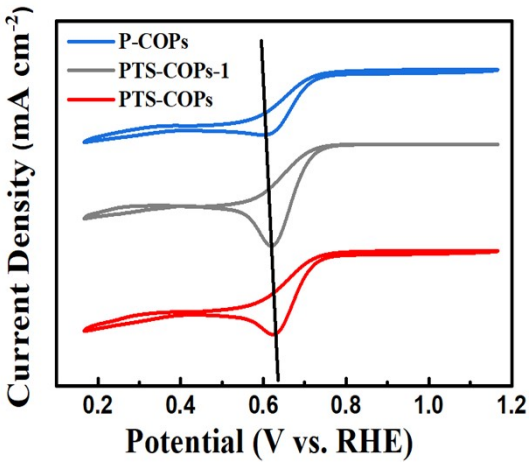

Figure S6. CV curves of the as-synthesized PTS-COPs, PTS-COPs-1 and P-COPs in O_2-saturated electrolyte.

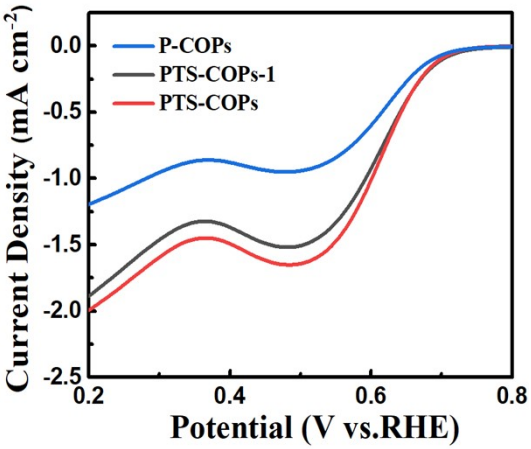

Figure S7. LSV curves of the as-synthesized PTS-COPs, PTS-COPs-1 and P-COPs at a rotation rate of 1600 rpm.

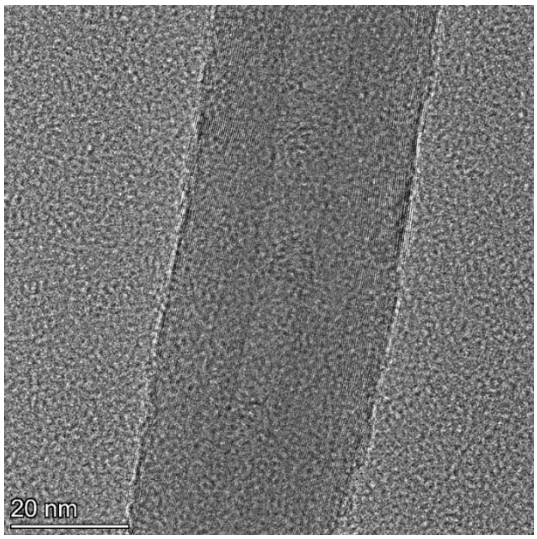

Figure S8. HRTEM image of the pristine MWCNTs with smooth and clean surface.

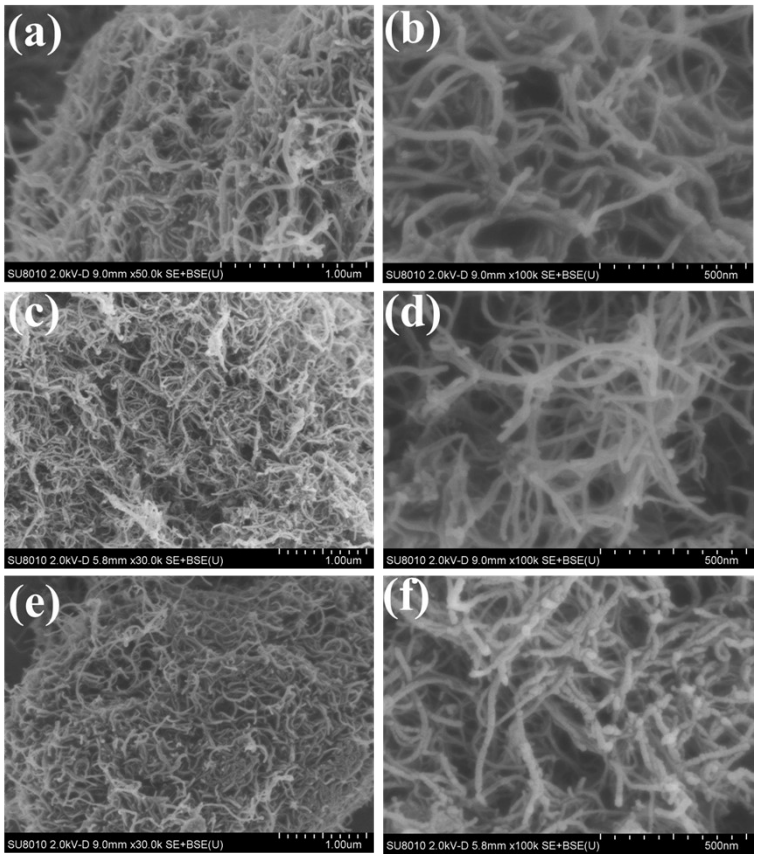

Figure S9. SEM images of (a,b) PTS-COPs@MWCNTs-0.5, (c,d) PTS-COPs@MWCNTs-1, and (e,f) PTS-COPs@MWCNTs-2, respectively.

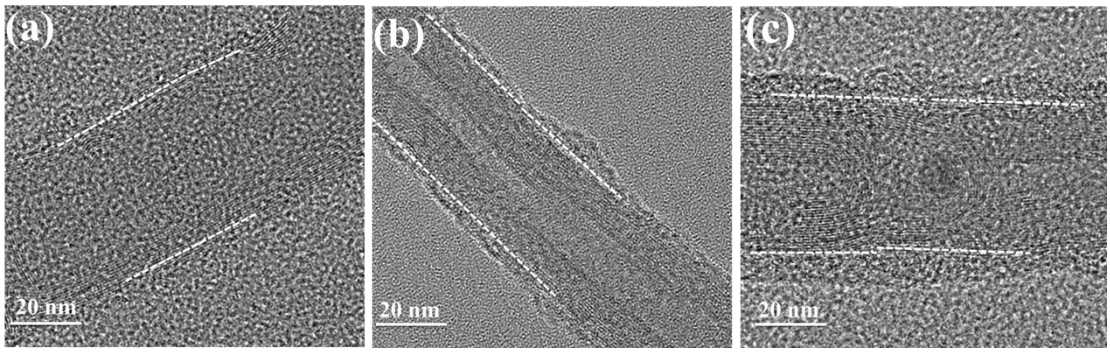

Figure S10. HRTEM images of (a) PTS-COPs@MWCNTs-0.5, (b) PTS-COPs@MWCNTs-1, and (c) PTS-COPs@MWCNTs-2, respectively.

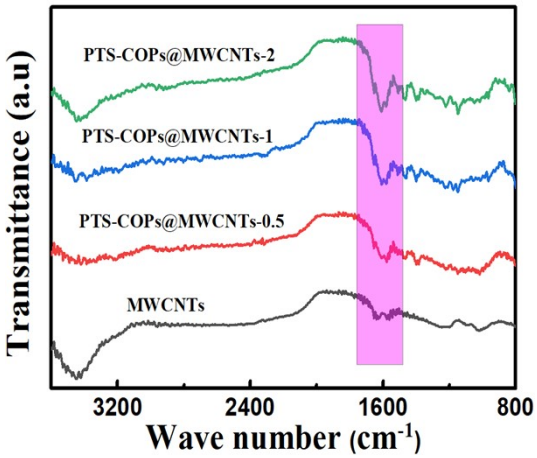

Figure S11. FTIR spectra of the as-synthesized PTS-COPs@MWCNTs-x (x = 0.5, 1 and 2) and pristine MWCNTs.

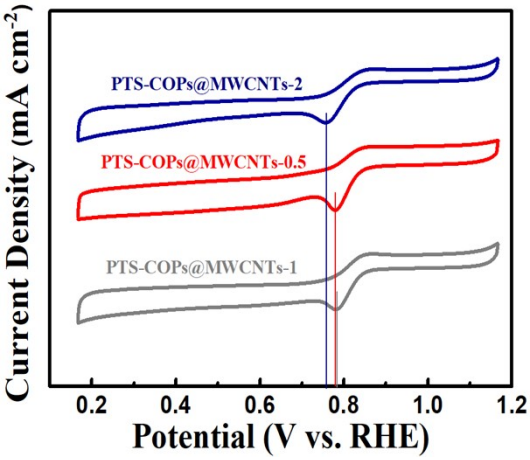

Figure S12. CV curves of the as-synthesized PTS-COPs@MWCNTs-x (x = 0.5, 1 and 2) in O_2-saturated electrolyte.

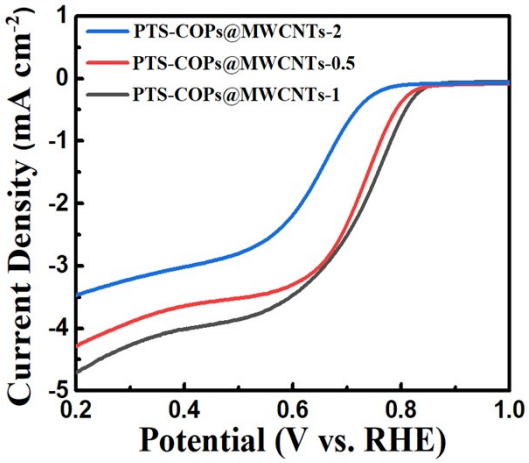

Figure S13. LSV curves of the as-synthesized PTS-COPs@MWCNTs-x (x = 0.5, 1 and 2) at a rotation rate of 1600 rpm.

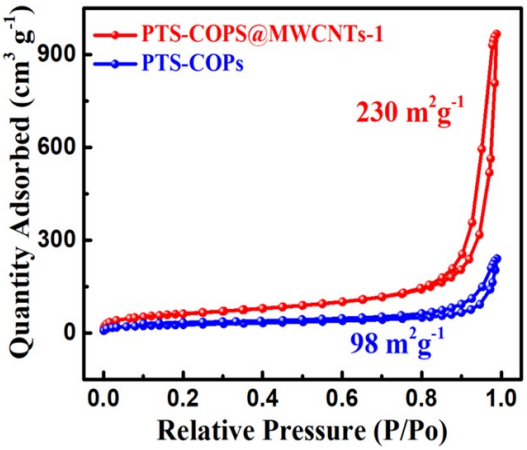

Figure S14. Nitrogen adsorption-desorption isotherm curves of PTS-COPs and PTS-COPs@MWCNTs-1.

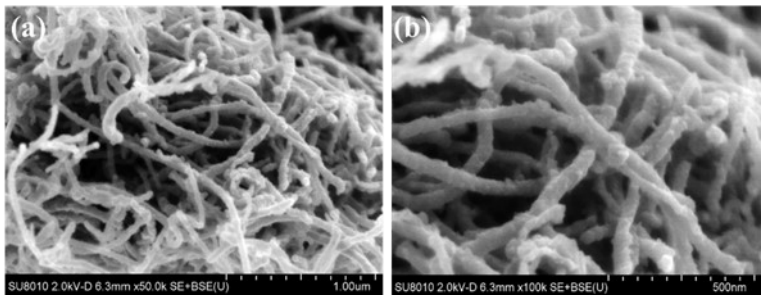

Figure S15. SEM images of the as-synthesized Co-PTS-COPs@MWCNTs.

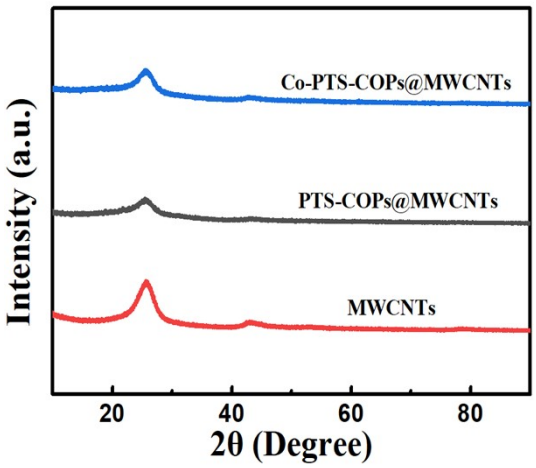

Figure S16. XRD patterns of the as-synthesized Co-PTS-COPs@MWCNTs, PTS-COPs@MWCNTs and pristine MWCNTs.

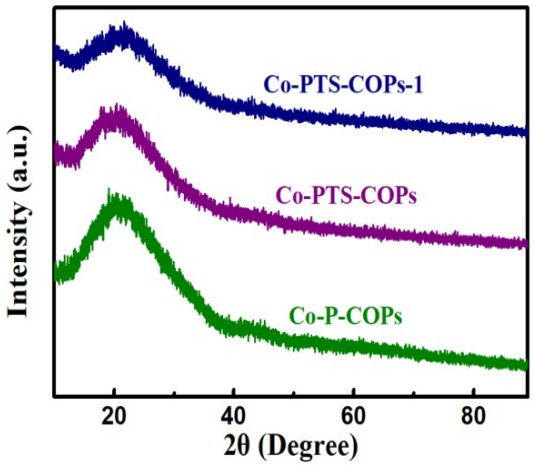

Figure S17. XRD patterns of the as-synthesized Co-PTS-COPs-1, Co-PTS-COPs and Co-P-COPs.

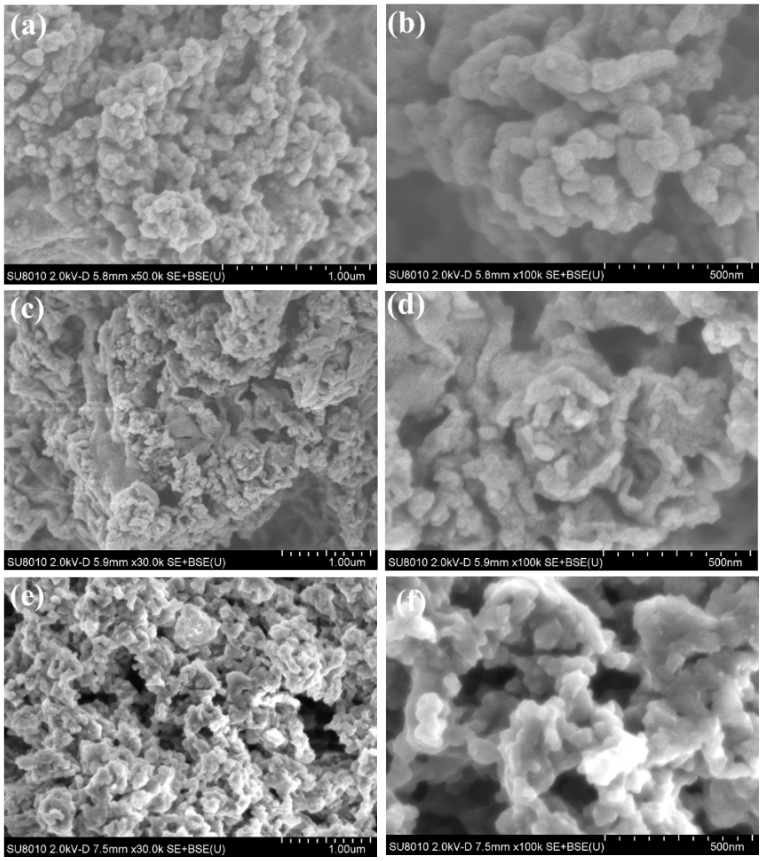

Figure S18. SEM images of the as-synthesized (a,b) Co-PTS-COPs-1, (c,d) Co-PTS-COPs and (e,f) Co-P-COPs.

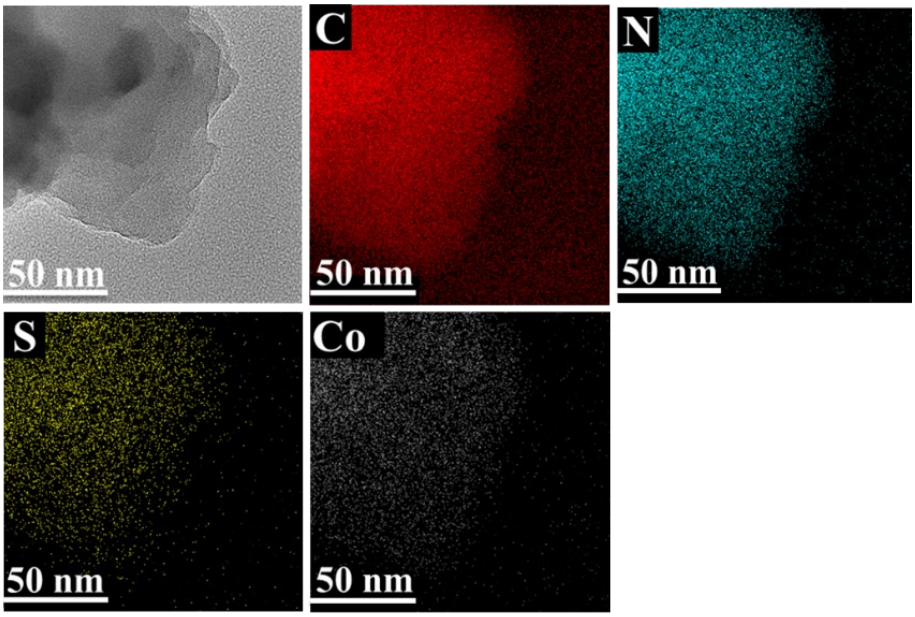

Figure S19. TEM image and EDX elemental mappings of the as-synthesized Co-PTS-COPs-1.

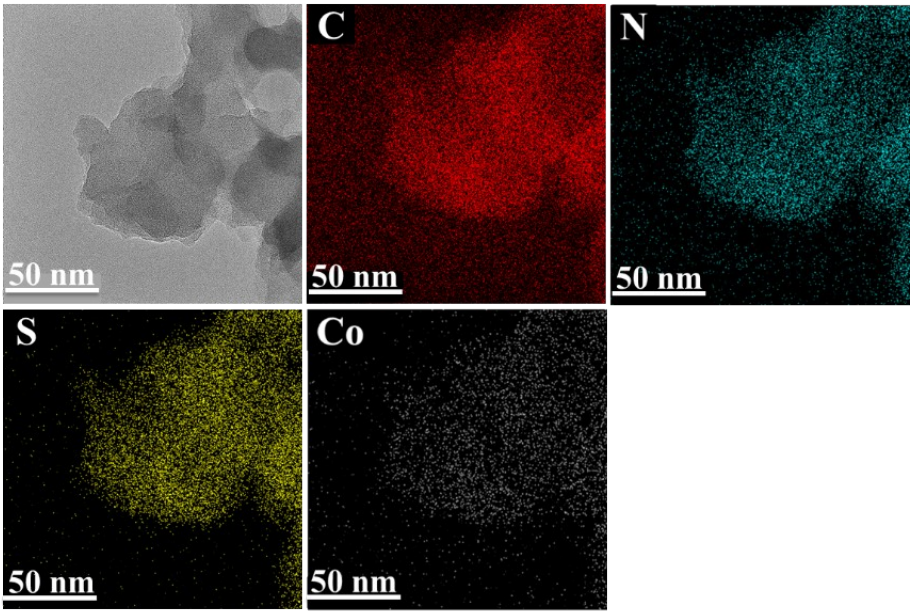

Figure S20. TEM image and EDX elemental mappings of the as-synthesized Co-PTS-COPs.

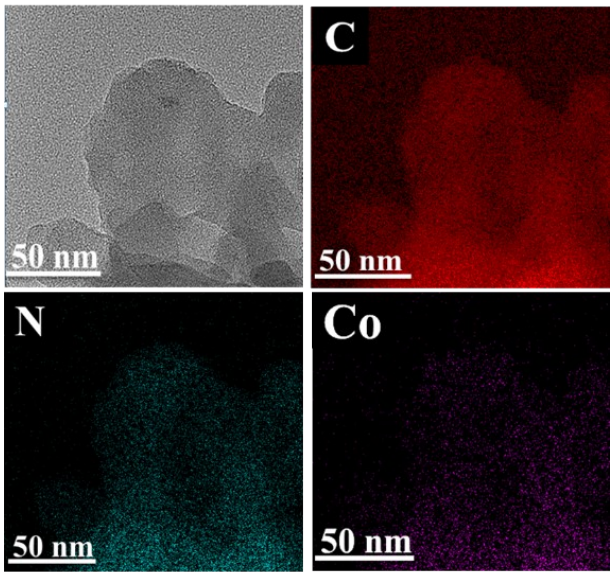

Figure S21. TEM image and EDX elemental mappings of the as-synthesized Co-P-COPs.

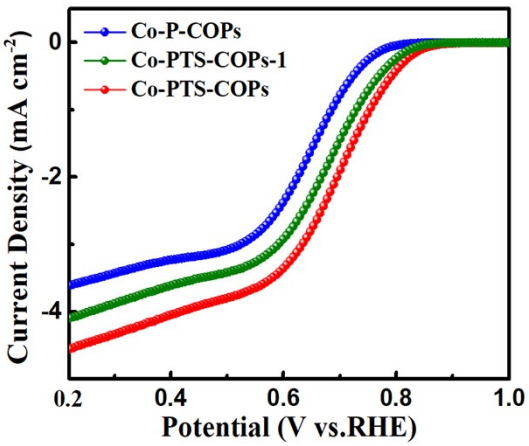

Figure S22. LSV curves of the as-synthesized Co-PTS-COPs-1, Co-PTS-COPs, and Co-P-COPs.

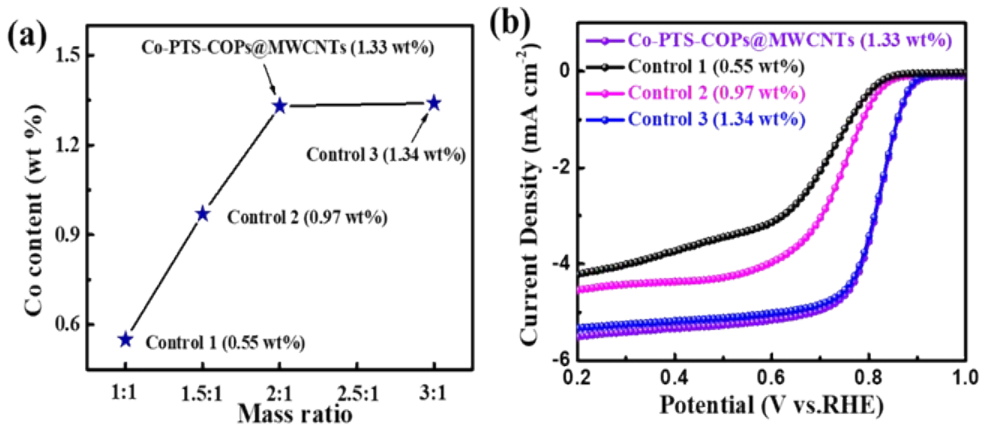

Figure S23. (a) The relationship between the mass ratio of Co precursor/PTS-COPs@MWCNTs-1 and the Co content measured by ICP-MS. (b) LSV curves of Co-PTS-COPs@MWCNTs and the as-synthesized control samples.

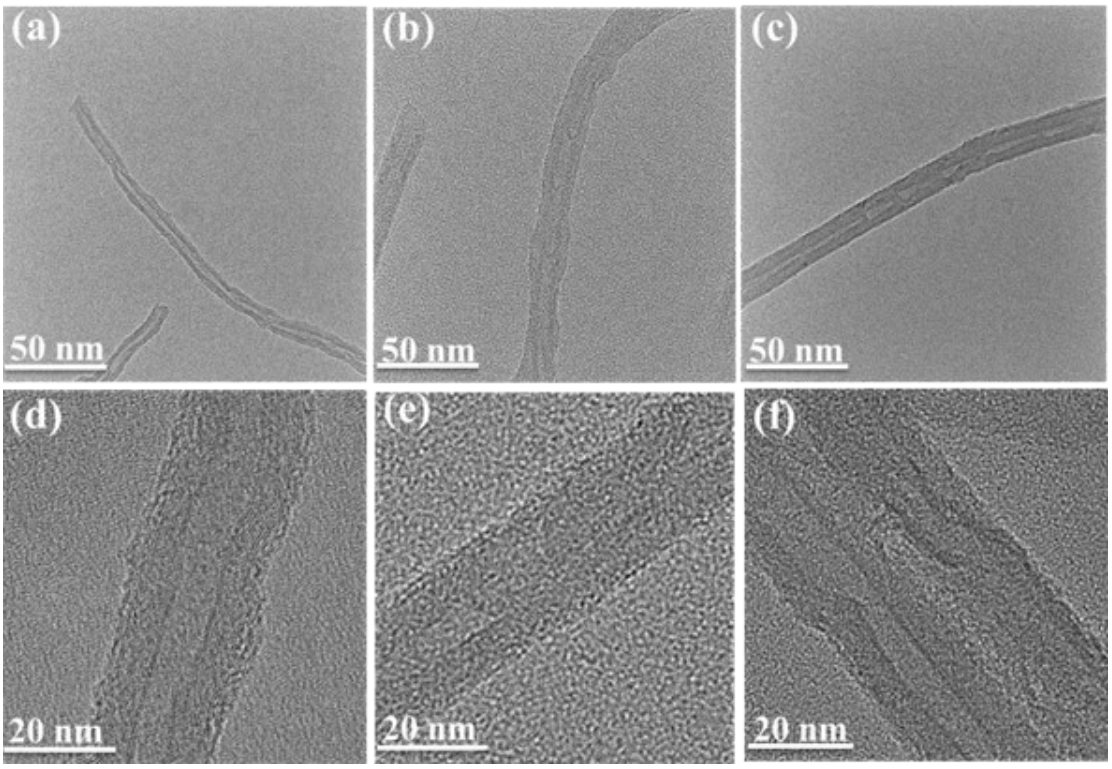

Figure S24. TEM (a-c) and HRTEM (d-f) images of the as-synthesized control samples with different Co content: control 1 (0.55 wt%) (a,d), control 2 (0.97 wt%) (b,e), and control 3 (1.34 wt%) (c,f).

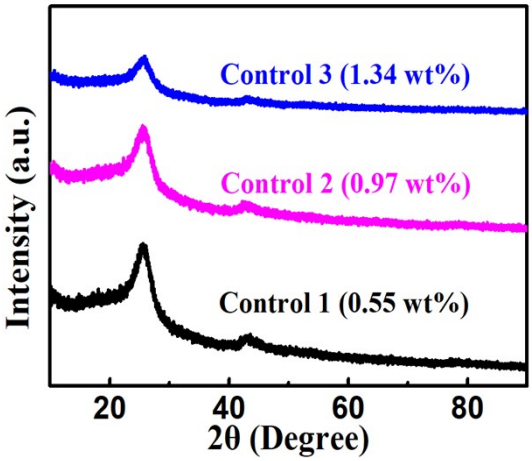

Figure S25. XRD patterns of the as-synthesized control samples with different Co content.

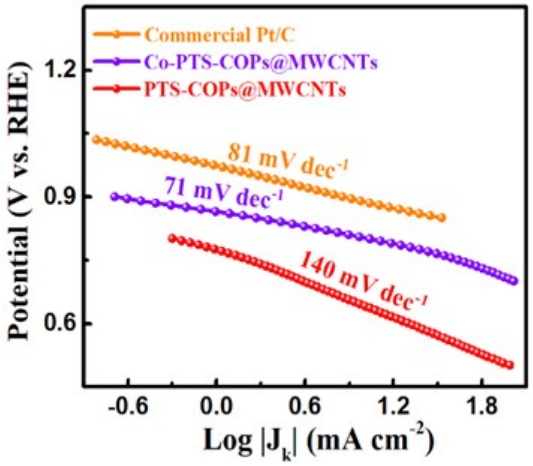

Figure S26. Tafel plots of Co-PTS-COPs@MWCNTs, PTS-COPs@MWCNTs and commercial Pt/C.

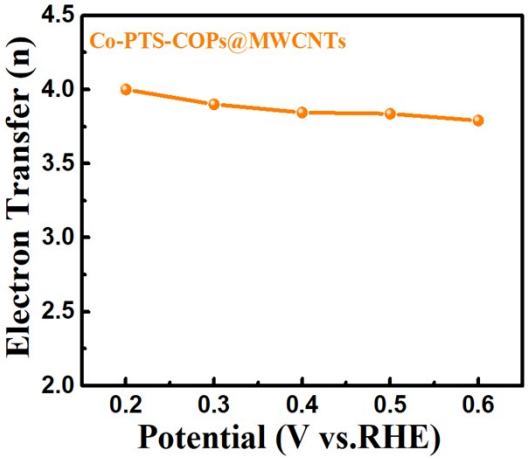

Figure S27. Electron transfer numbers at different potentials of the as-synthesized Co-PTS-COPs@MWCNTs.

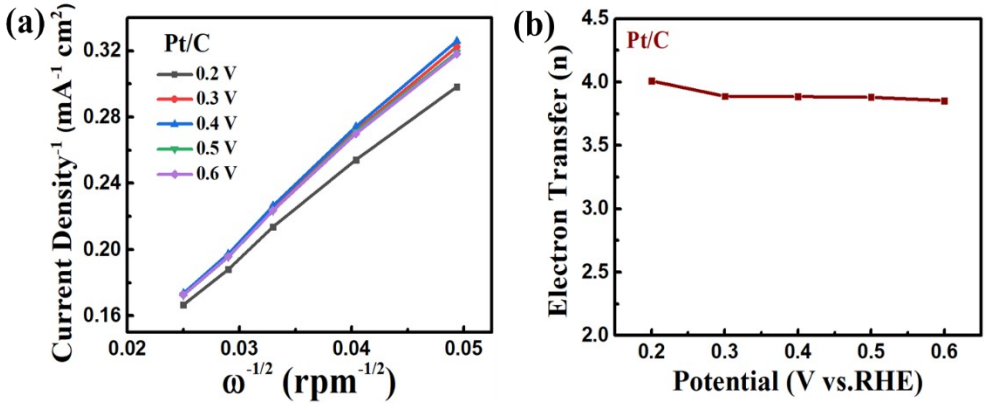

Figure S28. (a) K-L plot (j^{-1} vs. $\omega^{-1/2}$) and (b) electron transfer numbers at different potentials of commercial Pt/C catalyst.

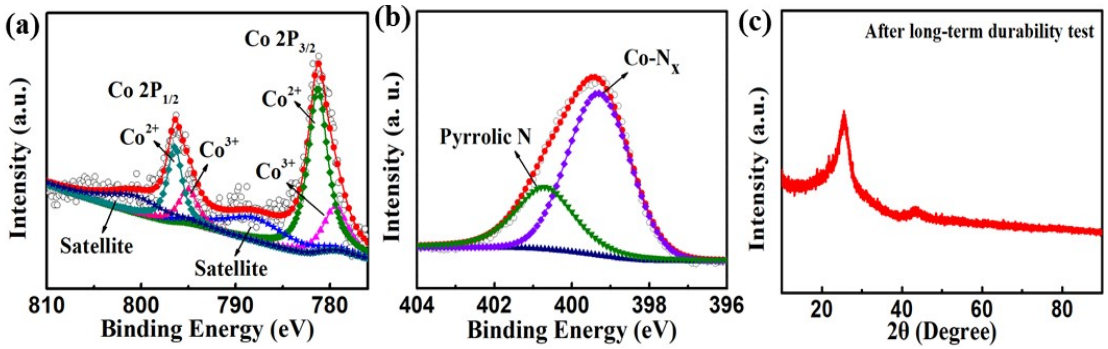

Figure S29. (a,b) High-resolution XPS spectra of Co 2p and N 1s, respectively, (c) XRD pattern of Co-PTS-COPs@MWCNTs after long-term durability test.

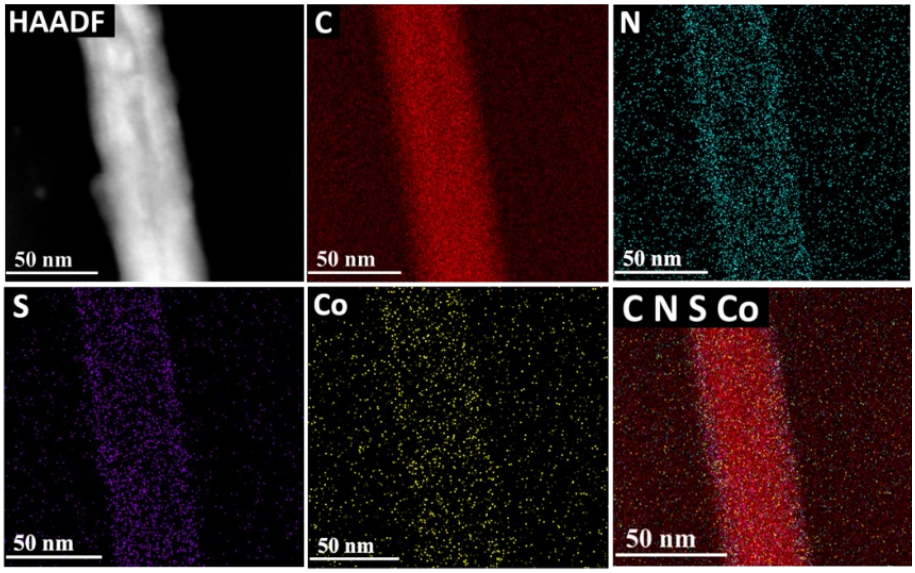

Figure S30. HADDF-STEM image and EDX elemental mappings of Co-PTS-COPs@MWCNTs after long-term durability test.

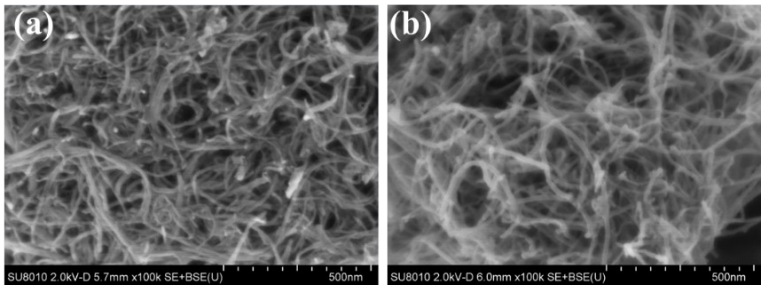

Figure S31. SEM images of the as-synthesized Fe-PTS-COPs@MWCNTs and Ni-PTS-COPs@MWCNTs.

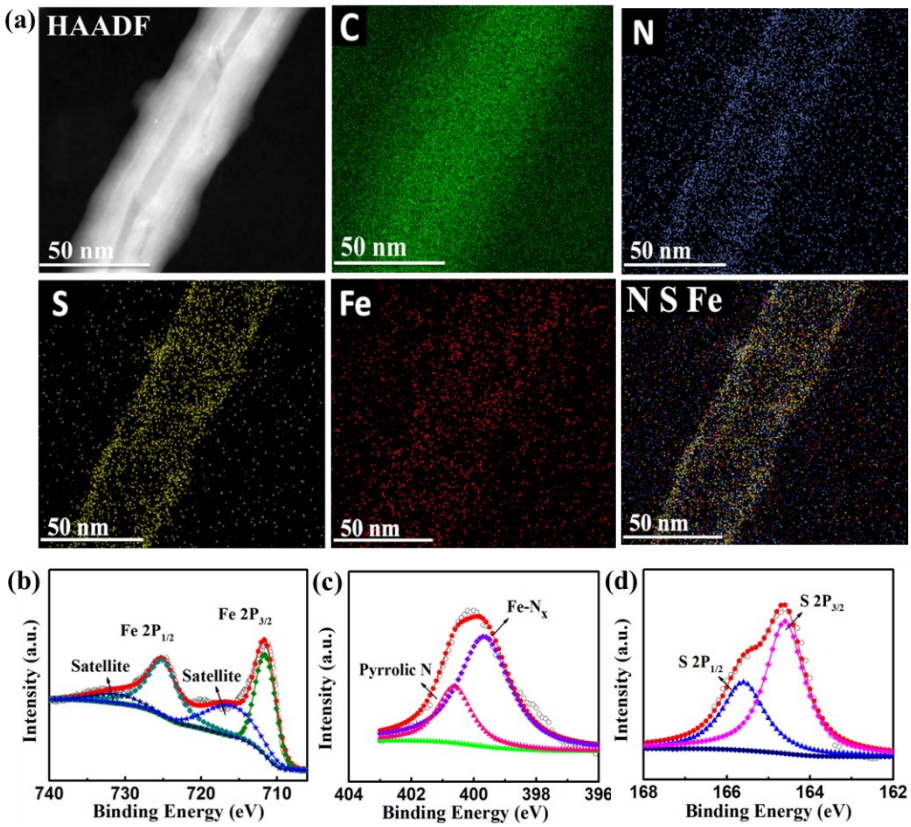

Figure S32. (a) HADDF-STEM image and EDX elemental mappings of Fe-PTS-COPs@MWCNTs. High-resolution XPS spectra of (b) Fe 2p, (c) N 1s and (d) S 2p of Fe-PTSCOPs@MWCNTs.

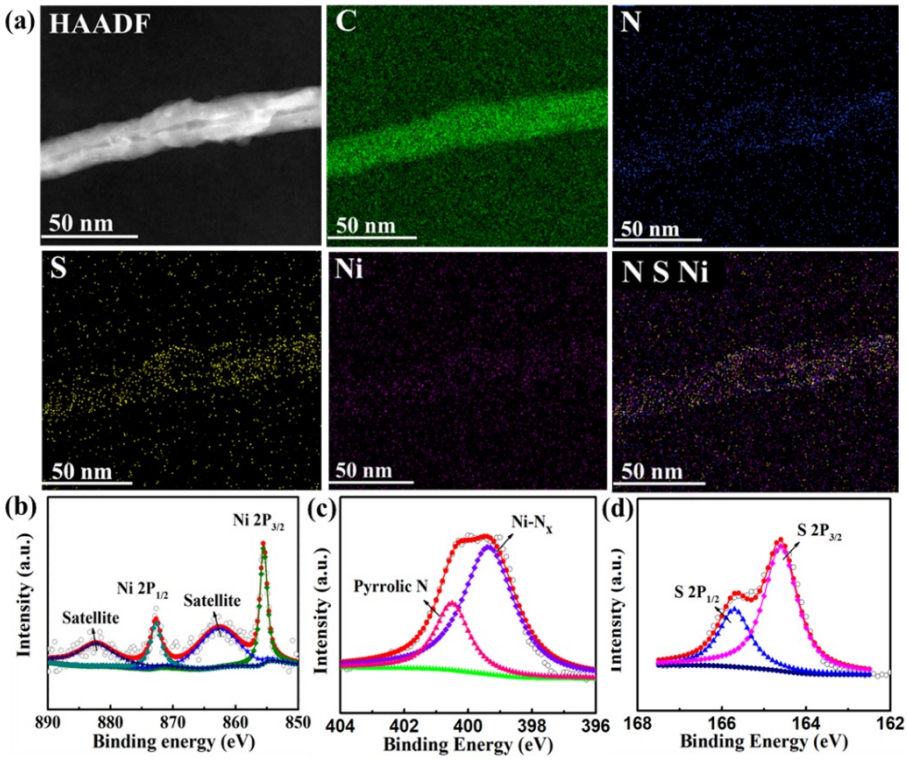

Figure S33. (a) HADDF-STEM image and EDX elemental mappings of Ni-PTS-COPs@MWCNTs. High-resolution XPS spectra of (b) Ni 2p, (c) N 1s and (d) S 2p of Ni-PTSCOPs@MWCNTs.

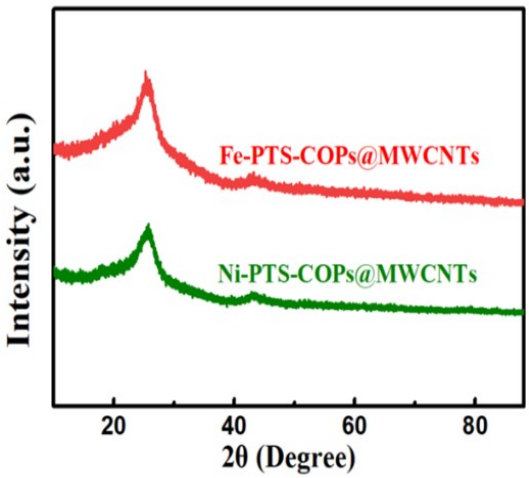

Figure S34. XRD patterns of the as-synthesized Fe-PTS-COPs@MWCNTs and Ni-PTS-COPs@MWCNTs.

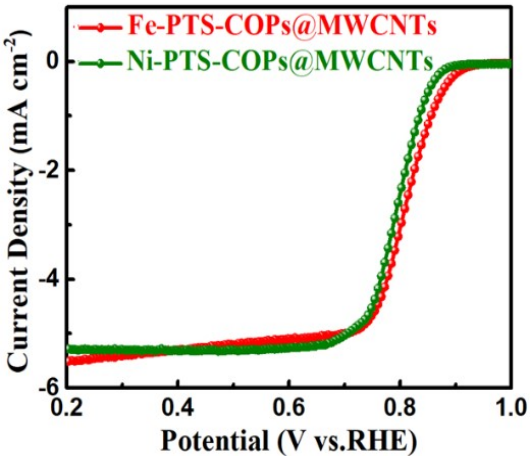

Figure S35. LSV curves of the as-synthesized Fe-PTS-COPs@MWCNTs and Ni-PTS-COPs@MWCNTs.

3. Tables

Table S1. Structural parameters extracted from the Co K-edge EXAFS fitting of Co-PTS-COPs@MWCNTs.

Sample	Path	N	R (Å)	σ^2 (10^{-3}Å^2)	ΔE_0 (eV)	R factor
Co-PTS-COPs@MWCNTs	Co-N	4.2	1.95	8.76	-2.83	0.0076

N: coordination number; R: interatomic distance; σ^2: Debye-Waller factor; ΔE_0: inner potential correction; R factor: goodness of the fitting.

Table S2. Comparison of various state-of-the-art carbon-based electrocatalysts towards ORR in alkaline solution.

Catalyst	E_{onset} (V vs. RHE)	$E_{1/2}$ (V vs. RHE)	J_d (mA cm^{-2})	n	Reference
Co-PTS-COPs@MWCNTs	**0.93**	**0.835**	**5.5**	**3.78-4.0**	**This Work**
Co/NC	0.9	0.82	3.94	3.7	*J. Mater. Chem. A*, **2020**, 8, 17266.
CNT@SAC-Co/NCP	0.90	0.870	5.3	3.85	*Adv. Funct. Mater.*, **2021**, 2103360.
Co-POC	0.85	0.83	5.0	—	*Adv. Mater.*, **2019**, 31, 1900592.
Co-ISAS/p-CN	0.95	0.838	5.1	3.9	*Adv. Mater.*, **2018**, 30, 1706508.
Co@N-C700	0.85	0.78	4.6	3.76-3.86	*Chem. Eng. J.*, **2021**, 421, 129719.
Co@MCM	0.95	0.86	4.9	3.7	*Energy Environ. Sci.*, **2018**, 11, 1980-1984.
Co-NCS-2	0.95	0.90	5.34	≈4	*Nano Energy*, **2021**, 87, 106153.
CoSAs-NPC	0.95	0.84	6.19	3.9	*Adv. Funct. Mater.*, **2021**, 31, 2010472.
Co/N/C	0.96	0.82	5.0	≈4	*Angew. Chem. Int. Ed.*, **2019**, 58, 5359.
CoP-DC	0.90	0.81	5.3	3.8	*Adv. Energy Mater.*, **2018**, 8, 1703623.
S-Co/N/C	0.99	0.86	6.0	3.85	*ACS Catal.*, **2021**, 11, 4498-4509.
Co-N_3C_1	0.904	0.824	4.5	—	*ACS Catal.* **2020**, 10, 5862-5870.
Co_1-HNC-500-850	0.90	0.827	4.98	3.81-3.96	*Adv. Mater.* **2020**, 32, 1906905.
Fe_1-HNC-500-850	0.93	0.842	5.8	3.88-3.99	*Adv. Mater.* **2020**, 32, 1906905.
Fe/N/S-PCNT	0.96	0.84	5.8	3.84	*J. Mater. Chem. A*, **2019**, 7, 1607-1615.